Expression and significance of histone methyltransferase SET domain containing 2 with histone H3 lysine 36 trimethylation in mouse hepatic oval cells differentiated into bile duct epithelial cells *in vitro*

LIQUAN JIN[1], ZITING SU[1], SHAN HUANG[1], YUNBO TAN[1], ISACK GEORGE MREMA[2] and YIMING CHEN[1]

[1]First Department of General Surgery, The First Affiliated Hospital of Dali University;
[2]Clinical Medical College, Dali University, Dali, Yunnan 671000, P.R. China

Received May 24, 2022; Accepted December 30, 2022

DOI: 10.3892/mmr.2023.12956

Abstract. The present study aimed to identify the function and expression of trimethylated protein histone H3 lysine 36 (H3K36)me3 and the upstream specific enzyme histone methyltransferase SET domain containing 2 (SETD2), during the differentiation of hepatic oval cells (HOCs) into cholangiocytes in mice following partial liver resection and fed with 2-acetamidofluorene. HOCs were isolated from Kunming male mice fed with 2-acetamidofluorene for 10 days. Their liver tissues were then isolated following partial liver resection and another week of 2-acetamidofluorene treatment. HOCs were collected following a two-step enzyme digestion procedure involving protease E and collagenase 4. The target cells were cultured in DMEM/F12 supplemented with 10 μg/ml EGF, 5 μg/ml stem cell growth factor and 5 μg/ml leukemia inhibitory factor. Target cells using the markers OV-6, CK-19, SETD2, H3K36me3, were detected with flow cytometry and immunofluorescence microscopy; reverse transcription-quantitative PCR and western blotting were used to quantify the protein levels of SETD2 and H3K36me3. The retrieved primary hepatocytes developed into cholangiocytes with increasing CK-19 and decreasing OV-6 expression in each subsequent passage, whereas the SETD2 and H3K36me3 levels gradually increased, suggesting the possible involvement of both of these factors in differentiation.

Correspondence to: Dr Yiming Chen, First Department of General Surgery, The First Affiliated Hospital of Dali University, 32 Carlsberg Avenue, Dali, Yunnan 671000, P.R. China
E-mail: drchenyiming@gmail.com

Key words: oval cell, bile duct epithelial cells, histone methyltransferase SET domain containing 2, histone H3 lysine 36 trimethylation, differentiation

Introduction

Bile duct disease, characterized by immune-mediated bile duct injury, inflammatory response and risks of fibrotic changes, is a chronic disease of the biliary system that causes cholestasis and secondary liver damage. Primary sclerosing cholangitis and primary biliary cholangitis are the two most common bile duct diseases in humans (1). The bipotential cells in the human liver can be differentiated into hepatocytes and bile duct epithelial cells (BDEs) (2), which are hepatic oval cells (HOCs). HOCs can be activated to proliferate and differentiate into mature hepatocytes and BDEs under certain conditions (3-6), and these are regarded as hepatic stem/progenitor cells. Activation of HOCs proliferation can be induced by a number of rodent models (7-9), but 2-acetylaminofluroene and partial hepatectomy (2-AAF/PH) is a traditional model to activate HOCs in rat liver (10). A number of study methods amass HOCs and show that the oval cells express hepatic oval cell-specific marker OV-6, BDEs marker CK-19 and hepatocyte lineage marker albumin and AFP (11). There still is a problem with inducting HOCs committed to other cells. However, the study of the directional differentiation of HOCs into BDEs is limited to explorations on cell morphology and methodology, still leaving its mechanism unclear (12,13). Therefore, studying the mechanism of directional differentiation of HOCs into BDEs may provide a new way for the treatment of bile duct diseases.

Epigenetics governs almost all aspects of the life of multicellular organisms, as it controls how differentiated cells achieve their unique phenotypes during development and differentiation, despite their uniform genetic makeup (with exceptions such as T cells and germ cells). Epigenetics involves chromatin remodeling, histone H3 lysine 36 (H3K36), DNA methylation (3) and non-coding RNA expression (4). For example, human primary hepatocytes have much more epigenetic regulation in terms of DNA methylation and histone modifications than human embryonic stem cell-derived hepatocytes due to their open chromatin structure, as represented by hypomethylation of CpG sites and permissive histone modifications (14). The human primary hepatocytes and inhibition of DNA methyltransferases during hepatic maturation induce

demethylation of the CpG sites of cytochrome P450 1A1 and cytochrome P450 1A2, thus leading to the upregulation of their transcription (14). Otherwise, in delta-like 1 protein hepatic stem/progenitor cells, 72 genes, including Cdkn2a and Sox4, are significantly upregulated after differentiation toward hepatocyte or cholangiocyte lineages as these genes exhibit bivalent domains within 2 kb of the transcription start site. The 2 kb is the 'bivalent domain', a distinctive histone modification signature characterized by repressive trimethylation of histone H3 at lysine 27 (H3K27me3) and active trimethylation of histone H3 at lysine 4 (H3K4me3) marks (15). Considerable emphasis should be placed on elucidating the epigenetic machinery underlying the terminal differentiation of HOCs.

A previous study has shown that histone H3 lysine 36 (H3K36), H3K36me3, can be catalyzed by histone methyltransferase SET domain containing 2 (SETD2) to undetected trimethylate in human liver cancer and liver tissues. It is only detected in the portal area of the liver and is positively correlated with CK-19, the bile duct epithelial marker and hepatocyte nuclear factor 1 (4). In this case, it is speculated that H3K36me3 might be associated with the differentiation of BDEs, but this has not been verified. Hence, the present study was performed to explore the role of SETD2 and H3K36me3 in the differentiation of HOCs and the possible mechanism by observing the expression changes of SETD2 and H3K36me3 in mouse HOCs differentiated into BDEs and analyzing its correlation with specific expression markers of liver oval cells OV-6 and BDEs CK-19.

Materials and methods

Animals. A total of 30 male SPF mice aged 6-8 weeks and weighing 20-25 g were collected from the Chinese Academy of Sciences' Kunming Laboratory Animal Center. A total of 15 mice were included in the experimental group and 15 were used as control group; every mouse was placed in a single cage alone. Since male mice have been as subject for liver regeneration in most researches, 6-8 week-old male mice were selected for all investigations. All mice were kept in a pathogen-free environment at the animal center of the Dali University School of Medicine (Dali, China). All animal tests were conducted in accordance with the rules of the Biomedical Research Ethics Committee of the School of Medicine at Dali University [approval number: SYXK(yunnan)2018-0002]. All the mice were kept with a 12-h light-dark cycle, a constant temperature of 25˚C and a humidity of 48%. Every attempt was made to reduce the suffering of mice during experiments, in order to record necessary information, animals behavior were observed and recorded every 24 h at least. The animals were not sacrificed until the successful cultivation of oval cells. During the 45-day duration of this investigation, 15 mice were sacrificed for the collection of HOCs following partial hepatectomy and two mice were found dead after the surgical procedure, possibly due to liver failure. At the end of the investigation, the remaining 15 mice were sacrificed by cervial dislocation after ether inhalation. During the investigation, the health and behavior of all the test animals were observed and documented. After administering general anesthesia with inhalation of 90% ether, which was administrated via wet cotton, cervical dislocation was employed for sacrifice. Mortality was declared 5 min after cervical dislocation and pupil dilation.

Surgical preparation. The animals received 10-mg/kg/day of 2-acetylaminofluorene (AAF; 2-AAF vegetable oil solution at a concentration of 0.2%) through gavage feeding for four consecutive days. On the seventh day, a PH (10) was conducted, followed by four further AAF treatments. On the tenth day after PH, the samples were obtained for the isolation of HOCs. Inhalation of 90% ether was used for general anesthesia.

Study design. A total of two experiments were performed following the presented sequence. HOCs were taken as the control group, while different differentiated BDEs were the experimental group.

Isolation of cells. The HOCs were extracted from mice treated with AAF/PH (10 mg/kg/day) and sacrificed on the tenth day after PH. The isolation and enrichment technique is briefly outlined in (6). The materials were digested with 0.10% collagenase IV (MilliporeSigma; cat. no. C4-BIOC) and 0.10% pronase E (MilliporeSigma; cat. no. 107433) before being separated and purified using density gradient centrifugation (150 x g for 10 min at 20˚C). The purified HOCs were cultivated in DMEM/F12 media with 10% calf serum and 1% double antibody (HyClone; Cytiva) together with penicillin and streptomycin (Beijing Solarbio Science & Technology Co., Ltd.).

Cell culture and induction differentiation. Sino Biological provided the neonatal calf serum (Thermo Scientific, Inc.) in DMEM-F12 media for cell culture, also the stem cell growth factor (SCF) and the leukemia inhibitory factor (LIF). On day 3, the initial HOCs generation was cultured in a DMEM-F12 culture mixture with 20% neonatal calf serum and on day 4, the DMEM-12 culturing media was supplemented with 20 ng/ml SCF, 10 ng/ml EGF and 10 ng/ml LIF. These cells were then cultivated in a cell incubator at 37˚C with 5% CO_2.

Cell morphology observation. The cell morphology and growth of both the experimental and the control group were examined using an inverted phase-contrast microscope every three days (x40 and x100 magnification), with the culture medium replaced and sub-cultured whenever necessary.

Flow cytometry analysis. Cultured primary cells and different differentiations of BDEs were detected using flow cytometry. Mouse monoclonal OV-6 antibody (1:100; Santa Cruz Biotechnology, Inc.; cat. no. sc-101863), rabbit anti-mouse CK-19 antibody (1:100; ABclonal Biotech Co., Ltd.; cat. no. A0247) and FITC conjugated donkey anti-rabbit antibody (1:100; ABclonal Biotech Co., Ltd.; cat. no. AS042) were used for flow cytometry detection. Santa Cruz Biotechnology, Inc., provided FITC-labeled goat anti-mouse antibodies (1:50; cat. no. sc-2010) and PE-labeled goat anti-rabbit antibodies (1:100; cat. no. sc-3739). Following centrifugation (120 x g for 5 min at 4˚C), sufficient cells were suspended in PBS buffer solution and the cell count was corrected to $1x10^5$/ml using Trypan blue (MilliporeSigma). The specific steps were to take a straw, put it into the culture flask, gently and repeatedly blow the cell

suspension to make the cells resuspended evenly, immediately absorb a little of the cell suspension, drop nine drops of cell suspension into another centrifuge tube, then one drop of trypan blue dye solution, mix them and leave the obtained solution for ~2-3 min. The counting plate was placed flat on the microscope stage and immediately 1-2 drops of stained cell suspension were added gently from the edge of the counting plate to fill the space between the counting plate and the cover glass. Microscopic observation (x40 and x100 magnification) showed that the cells were scattered evenly and the cell body of healthy cells was intact, transparent and non-pigmented. All the pigmented cells were unhealthy. The number of cells in the quadrants was then calculated. Only the left line and the top line were counted if the center line was touched, and the right line and the bottom line were not counted (i.e., only the cells touching two sides were counted). The calculation was using the following formula:

Cell count/ml of original suspension$=\frac{\text{Total number of cells in 4 large grids}}{4}$ x1,000 x diluted multiples. Cell suspensions from the same generation were deposited in three flow tubes, each consisting of a negative control group, an OV-6 group and a CK-19 group. The supernatant was collected and discarded after 8 min of (120 x g for 5 min at 4˚C) centrifugation. A corresponding primary antibody was added to each of the OV-6 and CK-19 group and incubated in the dark for 30 min before oscillation with 1 ml PBS buffer. Furthermore, before adding the corresponding secondary antibody for oscillation and incubating the antibody in a dark environment for 30 min before detection; an appropriate amount of cell washing solution was added and centrifuged at 120 x g at 4˚C for 8 min, the supernatant discarded and the cells washed twice repeatedly. The cells were resuspended with 100-200 μl PBS buffer. The blank tube and the homologous tube were tested first and then the OV-6 and CK-19 tube to be tested with a FlowSight® flow cytometer (model no. 00102107; Merck KGaA) and FlowJo10.8.1. (Becton, Dickinson & Company) to analyze the data. The late apoptosis + early apoptosis group (Q2+Q3) was used to calculate the apoptosis rate.

Immunofluorescence microscopy analysis. In vitro, primary isolated HOCs were grown and passaged 6-8 times. The cells were harvested and then incubated with rabbit anti-mouse CK19 (1:150; ABclonal Biotech Co., Ltd.; cat. no. A0247); and Cy3 conjugated goat anti-rabbit IgG (1:150; ABclonal Biotech Co., Ltd.; cat. no. AS007); anti-mouse OV-6 antibody (1:100; Santa Cruz Biotechnology, Inc.; cat. no. sc-101863); FCy3 conjugated goat anti-rabbit IgG (1:150; ABclonal Biotech Co., Ltd.; cat. no. AS007). Otherwise, HOCs, 5th and 8th BDEs were treated with rabbit anti-mouse SETD2 (1:100; ABclonal Biotech Co., Ltd.; cat. no. A11757); Cy3 conjugated goat anti-rabbit IgG (1:150; ABclonal Biotech Co., Ltd.; cat. no. AS007) and rabbit anti-H3K36me3 (1:500; ABclonal Biotech Co., Ltd.; cat. no. A2366; Cy3 conjugated goat anti-rabbit IgG (1:150; ABclonal Biotech Co., Ltd.; cat. no. AS007). HOCs were fixed in 4% paraformaldehyde for 15 min at 37˚C with oscillation and washed three times (each time 5 min) and ruptured within 30 min. The HOCs were then washed three times (5 min each time) with PBS at 37˚C with oscillation, followed by a 37˚C incubation in the dark for 20 min and then kept in a 4˚C refrigerator (in the dark) overnight. The following day, the primary antibody working solution was aspirated and washed three times with PBS and oscillation at 37˚C (5 min each time). The fluorescence-labeled goat anti-rabbit antibody was diluted 1:100 and incubated at 37˚C in the dark for 30 min. Finally, the solution was rinsed three times with PBS and oscillation (5 min each time) and was evaluated using an immunofluorescence detector (Olympus Corp.) and FlowJo10.8.1 software (Becton, Dickinson & Company), and mean fluorescence intensity was quantified using ImageJ v1.8.0 (National Institutes of Health).

Confocal microscope. In order to further verify the specific location of SETD2 and H3K36me3 distribution in cells, microscopic confocal observation was used. The third generation of BDEs was chosen as the experimental subject. A total of $1x10^5$ cells/ml cell suspension was prepared from DMEM/F12 medium containing 10% calf serum, and inoculated in confocal culture dishes with clean sterile cover slides, and cultured in a cell incubator at 37˚C with 5% CO_2 overnight. The slides were washed twice with PBS and 2 μl rabbit anti-mouse SETD2 (ABclonal Biotech Co., Ltd.; cat. no. A11757) and rabbit anti-H3K36me3 (ABclonal Biotech Co., Ltd.; cat. no. A2366) were added and incubated at room temperature for 40 min. The slides were washed twice with PBS and then 4 μl Cy3-conjugated goat anti-rabbit IgG (ABclonal Biotech Co., Ltd.; cat. no. AS007) was added at room temperature for 30 min. The slides were washed with PBS three times, before adding 2 μl DAPI dye solution for 5 min and washing with PBS another three times. The slides were sealed with a drop of 90% glycerin. An upper confocal microscope (Leica Microsystems, Inc.) was used to view the images and scan them using the Leica TCS SP8X system (Leica Microsystems, Inc.).

Endogenous nucleosome purification. To purify endogenous mono-nucleosomes, cell nuclei were isolated using hypotonic solution [5 mM HEPES, 10 mM KCl, 5 mM $MgCl_2$, 0.5 mM EDTA, 1 mM 2-mercaptoethanol, 0.4 mM phenylmethylsulfonyl fluoride (PMSF), 1 mM benzamidine and 1 mM sodium metabisulfite] followed by centrifugation at 2,700 x g for 5 min at 4˚C. Nuclei were re-suspended in 30 ml of buffer A (15 mM HEPES, 30 mM KCl, 3 mM $CaCl_2$, 3 mM $MgCl_2$, 1 mM 2-mercaptoethanol and 0.4 mM PMSF) and incubated with MNase at 4˚C for 15 min. Ca^{2+} ions were chelated by adding EDTA, EGTA and KCl to a final concentration of 5, 3 and 300 mM respectively to stop MNase reaction. FLAG-tagged H3-containing mono-nucleosomes were purified by incubating with αFLAG M2 beads for 2 h. Mono-nucleosomes were recovered from the beads by eluting with 3XFLAG peptide at 500 ng/ul in a buffer containing 20 mM HEPES, 1 mM EDTA, 10% Glycerol, 150 mM NaCl, 0.01% NP-40, 1 mM 2-mercaptoethanol and 0.4 mM PMSF. Finally, NaCl concentration was brought down to 50 mM using dialysis.

Histone protein analysis. Assays on mono-nucleosomes extracted from HOCs and BDEs was performed. Cells were harvested and washed twice with ice-cold PBS. To maintain the histone acetylation levels, PBS and subsequent buffers were added with 5 mM sodium butyrate. Cells were resuspended at 10^7 cells per ml in Triton Extraction Buffer (TEB;

PBS containing 0.5% Triton X 100 (v/v), 2 mM PMSF and 0.02% (w/v) NaN_3) and cells lysed for 10 min on ice with moderate shaking. To recover the nuclei, centrifugation at 650 x g for 10 min at 4˚C was performed. The supernatant was then removed and discarded. The nuclei were centrifuged at 650 x g for 10 min at 4˚C in half the volume of TEB. The pellet was resuspended to a density of $4x10^7$ nuclei per ml in 0.2 N HCl. The histones were acid extracted at 4˚C overnight. The debris was pelleted by centrifuging samples at 650 x g for 10 min at 4˚C. The supernatant (which contains the histone protein) was saved and the HCl neutralized with 2M NaOH at 1:10 of the supernatant volume. The Bradford test was used to determine the protein content, with the rabbit polyclonal anti-mouse H3K36me3 antibody (1:500; ABclonal Biotech Co., Ltd.; cat. no. A2366) and rabbit polyclonal anti-mouse Histone H3 antibody (1:500; ABclonal Biotech Co., Ltd.; cat. no. A2348) used as the primary antibody and horseradish peroxidase (HRP)-conjugated anti-rabbit (1:2,500; ABclonal Biotech Co., Ltd.; cat. no. AS014) employed as a secondary antibody. A 15% Bis-Tris gel, 1.0-mm thickness, was used for histone western blotting electrophoresis, and 5 μg sample was loaded in every lane, which includes the pre-stained protein standard. The gel was placed in MES SDS running buffer at 200 volts for 35 min. For effective histone protein retention, pore-sized porous nitrocellulose membranes with a diameter of 0.2 cm were used. The membrane was blocked with 5% BSA/0.1% TBST [50 mM Tris-HCl (pH 7.5) and 150 mM NaCl, 0.1%] for 1 h at room temperature (50 mM Tris-HCl, pH 7.5, 150 mM NaCl, 0.1%). The membrane was divided into strips and treated for 20 min at room temperature with primary antibody that had been diluted in blocking buffer (5% BSA/0.1% TBST). The membrane containing the primary antibody was stored for 16 h at 4˚C. The blots were briefly rinsed with 0.1% TBST, then the same buffer was used for two 5-min washes and two 10-min washes. After diluting the secondary antibody in 1% BSA/0.1% TBST, the membrane was incubated for 1 h at room temperature. In 0.1% TBST, the membrane was washed twice for 5 min and twice for 10 min. Clarity Western ECL blotting substrate was used for the study of histone proteins (Bio-Rad Laboratories, Inc.). Images were captured using autoradiography film or the Bio-Rad ChemidocMP (Bio-Rad Laboratories, Inc.) imaging equipment and the blots were analyzed using Bio-Rad Image Lab 5.0 software (Bio-Rad Laboratories, Inc.).

Reverse transcription-quantitative (RT-q) PCR. Cells were seeded into 6-well plates at $0.7x10^3$ cells/well. The total RNA was isolated according to the manufacturer's protocols using the RNAqueous micro kit (cat. no. AM 1931; Ambion; Thermo Fisher Scientific, Inc.). For cDNA synthesis, a high-capacity cDNA reverse transcription kit (cat. no. 4368814; Applied Biosystems; Thermo Fisher Scientific, Inc.) was used according to the manufacturer's protocols. The ABI Prism 7300 sequence detection system (Applied Biosystems; Thermo Fisher Scientific, Inc.) was used to run qPCR for SETD2 (Assay ID: Rn00562048 m1) in accordance with the instructions of the manufacturer using the ChamQ SYBR qPCR Master Mix (cat. no. Q311-02; Vazyme Biotech, Co., Ltd.). Endogenous control was GAPDH; mSETD2: Sense 5'-3'CATAGCTGTGAACCA AACTGTGA; antisense 5'-3' TAATTCTGAGCCTGAAGG AACTA; GAPDH: Sense 5'-3'AGGTCGGTGTGAACGGAT TTG; antisense 5'-3'TGTAGACCATGTAGTTGAGGTCA. The total volume of each reaction was 20 μl. The PCR thermocycling conditions were as follows: 95˚C for 5 min, with 40 cycles of 95˚C for 10 sec, 58˚C for 30 sec and 70˚C for 10 sec. In a 20-μl reaction volume, all samples were run in triplicate and the results were calculated as threshold cycle (CT) values. The expression levels were calculated using delta CT. The data were determined as the mean of three independent measurements and the relative mRNA expression level was determined with the $2^{-\Delta\Delta Cq}$ model (16).

Western blot analysis. For full lapping cleavage, 0.020 g of cells were mixed with RIPA lysis (Beyotime Institute of Biotechnology) and supernatant was obtained after centrifugation at 1,400 x g at 4˚C for 20 min. The protein content was determined using the BCA method (Tiangen Biotech Co., Ltd.) and protein samples were generated. A 10% SDS-PAGE gel was generated for sample separation. A 100-ng quantity of total protein extracts were loaded per lane, After electrophoresis, the protein extracts were transferred onto PVDF membranes, and then the PVDF membranes were blocked with blocking reagent (5% skimmed dried milk) for 1 h at room temperature. The primary antibodies were added and incubated overnight at 4˚C in a shaking table: Rabbit polyclonal anti-mouse SETD2 antibody (1:1,000; ABclonal Biotech Co., Ltd.; cat. no. A11757) and rabbit polyclonal anti-mouse Histone H3 antibody (1:500; ABclonal Biotech Co., Ltd.; cat. no. A2348). The TBST membrane was cleaned. Following incubation with HRP-conjugated anti-rabbit antibodies (1:2,500; ABclonal Biotech Co., Ltd.; cat. no. AS014) for 1 h at room temperature, the TBST membrane was washed and an ECL kit (Fdbio Science) development was used; a Bio-Rad Laboratories, Inc. gel imaging system was employed and the gray value of each strip was analyzed using ImageJ 1.6 software (National Institutes of Health). The target protein to anti-Histone H3 was used as an internal reference.

Label-free proteomic analysis. To clarify how functional proteins alter throughout the directed differentiation of HOCs into BDEs, a thorough proteomics method was used for hepatica oval cells and BDEs to determine the functional protein connections between HOCs and BDEs. HOCs were chosen as the control group and cell shape changed with each generation, including cells in the fourth and eighth generations of the experimental group. The first stage of cell sample processing was as follows: The cells were trypsinized and harvested. For $1x10^6$ cells, 400 μl lysis buffer (7M urea, 2M thiourea, 0.1% PMSF, a protease inhibitor, 65 mM DTT) was added and the sample sonicated on ice. Ultrasound conditions were: 70-75 W ultrasound, 5 sec ultrasound, 10 sec rest and 3-5 times ultrasound after 40 min on ice. The supernatant was centrifuged for 30 min at 14,00 x g and 4˚C, which is a two-step process to protein quantification. The concentration of isolated protein was determined using the Bradford method. The sample was diluted with lysis buffer until the final concentration was within the range of the standard. The diluted sample and standard (10 μl; dissolved with BSA into a series of concentrations of the standard protein in lysis buffer) and 300 μl of protein quantitative dye (Coomassie

Brilliant Blue G-250; cat. no. B802204; Shanghai Macklin Biochemical, Co., Ltd.) were reacted in the dark for 15-20 min before measuring the absorbance of the standard and sample at 595 nm with a microplate reader. A standard curve was obtained based on the relationship between the absorbance and concentration of each standard tube. SDS-PAGE electrophoresis was accomplished in three phases. To control the cell sample volume: 2X Loading buffer volume (5:1) was mixed well and then the proteins denatured at 100˚C for 8 min. In general, the maximum sample volume for each electrophoresis lane was 30 μl, the lowest amount of protein loaded in each electrophoresis lane (each protein band) was 0.1 μg (Coomassie brilliant blue staining) to 2 ng (silver staining) and the maximum protein amount (protein mixture) was 20-40 μg; 150-160 V was used for 1 h at 90˚C. Enzymatic cleavage of peptides involved four stages. The samples were separated into five divisions using Coomassie brilliant blue dyed gel. Then, the gel was cut into 1-2 mm^2 films with a knife and placed in tiny vials. To soak, 200 μl of the decolorizing solution was added and shaken for 10 min and was then removed. The steps were repeated 1-2 times until the blue color faded. Acetonitrile (200 μl) was added and the waste solution discarded. A total of 100 μl LDTT reduction solution was added for 30 min at 56˚C, then the waste liquid discarded and 200 μl acetonitrile added for 5-10 min of dehydration. Iodoacetamide (100 μl) was added for alkylation in the dark for 30 min, followed by 100 μl of decolorization solution, washing with water for 5-10 min, acetonitrile (100 μl) was added, the waste solution discarded and the sample was washed three times with water and acetonitrile before freeze-drying for 20 min. Then, 50 μl of enzyme solution (0.01 ug/μl) was added and left at 4˚C for 30 min. After that, 50-100 μl of enzymolysis buffer (25 mM NH_4HCO_3) was added and when the enzyme solution was entirely absorbed the gel was completely immersed and maintained at 37˚C for at least 15 h or overnight. Extract I (100 μl; 5% TFA) was added and heated it for 1 h in a water bath at 40˚C and sonicated for 3 min at 30 min at 20 kHz in 40˚C. The extract was aspirated into another clean tube, freeze-dried and then 100 μl of Extract II (50% acetonitrile; 2.5% TFA) added to block the gel which was incubated at 30˚C for 1 h, then sonicated for 3 min at 20 kHz in 40˚C. The extracts were combined, blown to dry the acetonitrile with nitrogen, and freeze-dried. TFA solution (5-10 μl; 0.1%) was added, thoroughly stirred and analyzed using mass spectrometry. The gel glass plate was removed from the electrophoresis device and stained for 1 h with Coomassie brilliant blue before distaining. Generally, there are five steps involved in performing Liquid Chromatography with tandem mass spectrometry (LC-MS-MS). In the present study, the high pH reverse phase separation fractions were reconstituted with 20 l of 2% methanol and 0.1% formic acid, which were then centrifuged at 13,00 x g for 10 min at 4˚C and aspirated. The supernatant was loaded. The sample volume was 10 μl and it was loaded at a loading flow rate of 350 nl/min for 15 min using the sandwich approach. The flow rate of separation was 350 nl/min and the separation gradient was as shown in Table I.

The raw data were processed using the Proteome Discoverer 2.5.0.400 software (Thermo Fisher Scientific, Inc.). Protein identification analysis was performed based on the data available in the UniProt protein sequence database for the Homo sapiens Proteome 2020_05 with 75,069 entries and a common contaminant database from MaxQuant (version 1.6.2.6, Max Planck Institute of Biochemistry). A heatmap was visualized using the 'heatmap.2' function from the 'gplots' R-package and R language (https://www.r-project.org/) 'cor' function to compute correlation proteins for correlation analysis. Metascape, a web-based resource (http://metascape.org), was used to conduct Gene Ontology (GO) analysis and the Kyoto Encyclopedia of Genes and Genomes (KEGG) Orthology-Based Annotation System (KOBAS) online analysis tool (http://kobas.cbi.pku.edu.cn/) was used to perform KEGG pathway analyses. Database enrichment analysis was performed using the UniProtKB database (Release 2016 10). GO enrichment included three ontologies [biological process (BP), molecular function (MF), and cellular component (CC)]. In addition, protein-protein interaction (PPI) analysis was performed using STRING software (http://string-db.org/).

Table I. Separation gradient analysis by liquid chromatography with tandem mass spectrometry.

Time, min	Mobile phase B ratio, %
0	4
5	15
40	25
65	35
70	95
82	95
85	4
90	4

Mobile phase A: 100% ultrapure water, 0.1% formic acid. Mobile phase B: 100% acetonitrile, 0.1% formic acid.

Statistical analysis. Data were analyzed with one-way ANOVA for comparisons of multiple groups followed by Tukey's multiple comparisons test using Prism (version 7; GraphPad Software; Dotmatics). All data were assessed for distribution normality using the Shapiro-Wilk test. The results were expressed as the mean ± standard deviation. $P<0.05$ was considered to indicate a statistically significant difference.

Results

HOCs morphological features in the original generation and differentiation into BDEs. A modified two-step enzyme digestion method established proliferation of HOCs in the mouse model using the 2-AAF/PH method. After the separation of HOCs under light microscopy, the cells were found to be oval and the cell volume was small, with large nuclear/cytoplasmic ratios. Bulkier oval cells (Fig. 1A) were also observed. However, rapid cell growth of the first generation typical colony formation was observed after being combined with the culture medium containing cytokines for 3 days (Fig. 1B). During the process, the nucleus was gradually increased (Fig. 1C). When the cell culture passed to the 2nd and 3rd generation, a number of cells were irregular-shaped, with a large cell volume and a high cell quality. Some cells had apparent nuclei

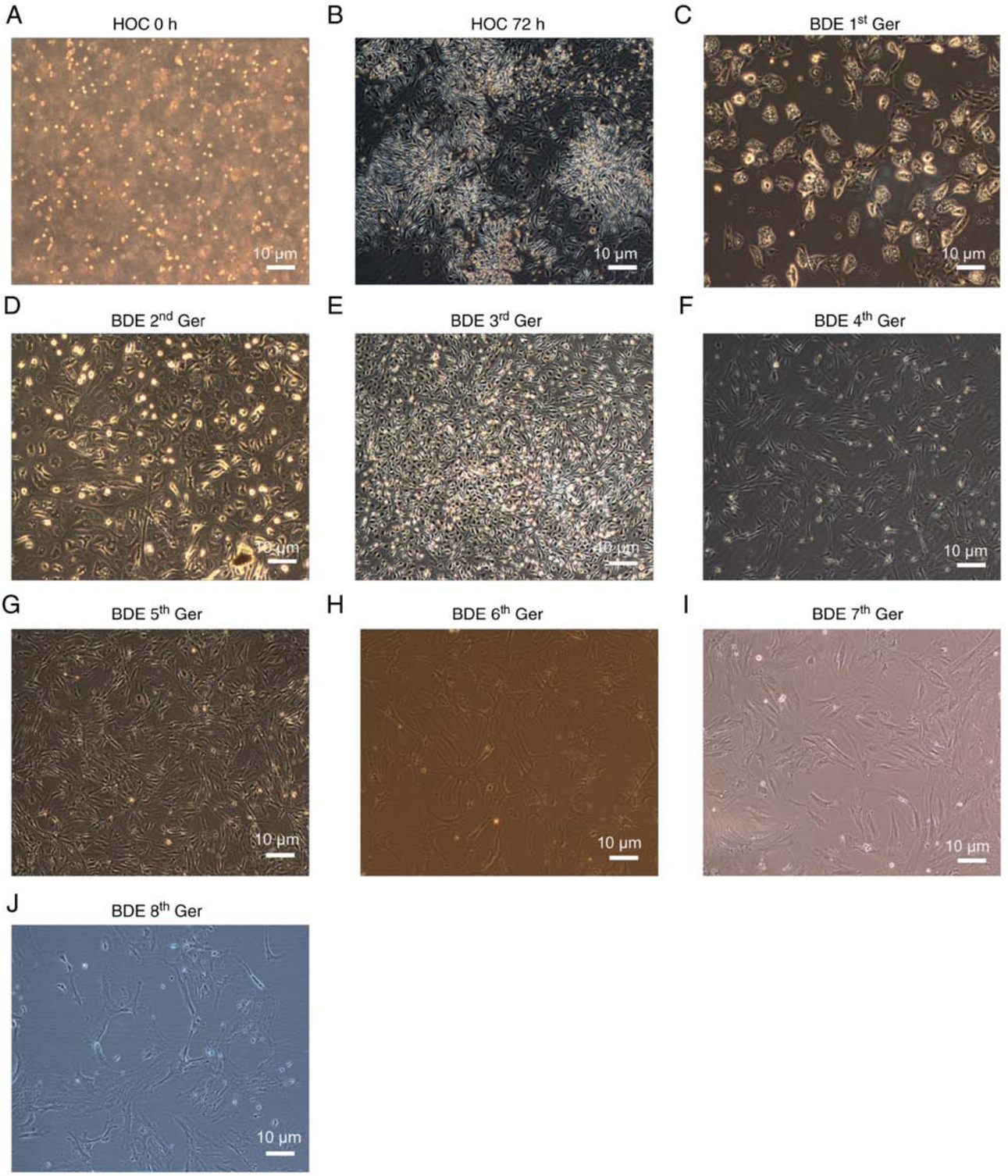

Figure 1. HOCs morphological features in the original generation and differentiation into BDEs with 10 μg EGF + 5 μg stem cell growth factor + 5 μg leukemia inhibitory factor. (A-J) Images of cell morphology under inverted microscope (scale bar, 10 μm). HOCs, hepatic oval cells; BDEs, bile duct epithelial cells.

(Fig. 1D and E). The 4th and 5th generation of BDEs was differentiated, the cell mass was significantly enlarged and the cell volume was increased gradually (Fig. 1F and G). When the passage to 6, 7 and 8th generation of BDEs was induced and differentiated, changes were found in bile duct epithelium and multiple 'pseudopodia'-like growth and the induced HOCs were not layered at the bottom of the cell culture flask, but presented a certain three-dimensional structure (Fig. 1H-J). To confirm that the isolated and differentiated cells were HOCs and BDEs, OV-6 and CK-19 were used in immunofluorescence microscopy and flow cytometry, which marked BDEs and HOCs. As the results revealed, CK-19 positive cells were gradually increased while, on the contrary, the OV-6 positive cells showed a significant decrease from 1st bile duct epithelium cells generation. ($P<0.05$; Fig. 2Aa-e; Fig. 2Ba-e and Table II; detailed flow cytometry shown in Fig. S1).

Table II. Results of OV-6 and CK19 flow in different generations of BDEs induced *in vitro* mouse HOCs differentiation.

Molecular markers	Number of cases	Cell generations		
		HOC	BDE 5th Ger	BDE 8th Ger
OV-6	3	76.60±3.14	37.10±3.21[a]	1.65±0.14[a,b]
CK-19	3	6.15±4.29	53.24±6.60[a]	96.38±1.23[a,b]

[a]P<0.001 vs. HOCs; [b]P<0.001 vs. 5th generation BDEs cells. BDEs, bile duct epithelial cells; HOCs, hepatic oval cells.

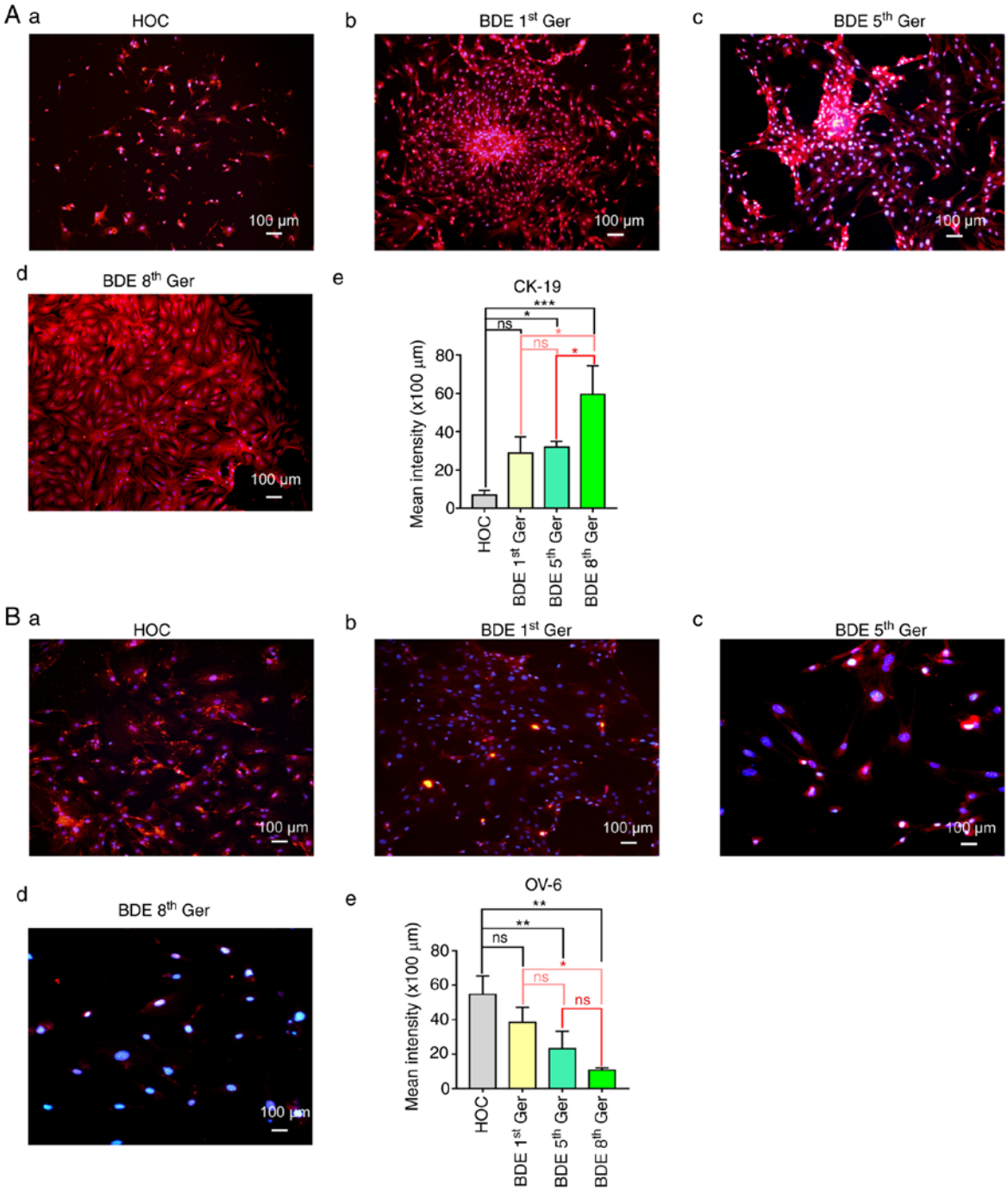

Figure 2. Representative images of immunofluorescence staining for CK-19 (Aa-d) and OV-6 (Ba-d) with primary hepatic oocytes, with induced differentiation of BDEs represented by the red and green fluorescence and DAPI used as the counterstain (scale bar, 100 μm) and (Ae and Be) quantification of red and green fluorescence. Data presented as mean ± standard deviation, n=3. Black * indicates significant differences vs. primary HOCs; pink * indicates significant differences vs. BDEs 1st Ger and red * indicates significant differences vs. BDEs 5th Ger. ns, P>0.05; *P<0.05; **P<0.01; ***P<0.005. HOCs, hepatic oval cells; BDEs, bile duct epithelial cells; Ger, generation.

Changes of SETD2/H3K36me3 expression in mice liver oval cells induced to differentiate into BDEs *in vitro*. Although SETD2 and H3K36me3 have been confirmed to have significant effects on cell differentiation, such as in hematopoietic stem cells (17) and bone marrow mesenchymal stem cells (18), changes in the expression of SETD2 and H3K36me3 during HOCs differentiation into BDEs have not been examined, to the best of the authors' knowledge. In order to investigate the role of SETD2 and H3K36me3, HOCs were induced to be differentiated into BDEs *in vitro*. First, it was found through culture of HOCs and induced differentiation of BDEs that the general shapes of cells were not so different on the two continuous passages, indicating that the markers expression might be identical between the two neighboring passages. Hence, passages 5 and 8, which were distinguishable on the shapes as the experimental targets were selected to explore the key proteins expression. Immunofluorescence analysis of the cell location and expression was conducted with SETD2 and H3K36me3 in primary oval cells obtained from liver samples having undergone 2AAF/PH and committed differentiation bile duct cell passages 5 and 8 using EGF 20 μg/l + SCF 10 μg/l + LIF 10 μg/l protocol. It was confirmed that SETD2 and H3K36me3 were, in fact, observed at all time points during committed differentiation ($P<0.05$; Fig. 3Aa-d and Ba-d). However, SETD2 was expressed in the cell nucleus and cell cytoplasm and had increased significantly since the primary generation (Fig. 3Aa-d). By contrast, H3K36me3 was mainly expressed in the cell nucleus as the differentiation process gradually increased (Fig. 3Ba-d). To confirm the immunofluorescence results, Confocal microscopy was used to test the SETD2 and H3K36me3 cell location in the third generation of BDEs. The conclusion seemed to be that the immunofluorescence showed that SETD2 was mainly expressed in the nucleus and cytoplasm, while H3K36me3 was mainly expressed in the nucleus (Fig. 3Ca and b). Next, RTqPCR analysis of cDNA obtained from the cells differentiation over generations clarified that SETD2 mRNA was gradually increasing and being stabilized during the progress of HOCs differentiation into mature BDEs (Fig. 3D). Western blotting was used to test SETD2 and H3K36me3 proteins in primary oval cells obtained from liver samples which had undergone 2AAF/PH and differentiated BDEs generation 5 and 8 using EGF 20 μg/l + SCF 10 μg/l + LIF 10 μg/l protocol (Fig. 3E and F). Analysis of these protein levels in Fig. 3E revealed that the expression of SETD2 and H3K36me3 in 3rd generation BDEs, compared to that of mice primary HOCs, was increased by ~35%. In the 5 and 8th generation mature BDEs, both were increased by ~75% and tended to be stabilized.

Label-free test of the hub proteins during the differentiation of HOCs into BDEs. As expected, SETD2 and H3K36me3 presented significantly increased expression during the progress of HOCs differentiation into BDEs. To further confirm the mechanism of both SETD2 and H3K36me3 increasing in the presence of HOCs committed into BDEs, a protein chip was performed to search deferentially expressed proteins using the label-free technology method, which is a widely used method for protein identification and which couples prefractionation of protein samples by one-dimensional PAGE with LC/MS/MS (16). Following this method, the protein detection of the HOCs, the 4th generation BDEs and the 8th generation BDEs was performed. Each sample was repeated three times.

On the basis of the label-free LC-MS/MS data, a total 162,294 unique peptides and 15,065 proteins were identified and 5,210 proteins were quantified on the basis of the identification of one or more unique peptides across all three biological replicates in each group. The quality assessment is shown in Fig. S2. The correlation analysis for proteins between BDEs 4/8th Ger and HOCs groups is shown in Fig. S3 (HOCs vs. BDEs 4th Ger, HOCs vs. BDEs 8th Ger and BDEs 4th Ger vs. BDEs 4th Ger; Pearson correlation <1). The fold change >2.0 or <0.5 in relative abundance and P-value <0.05 were seen as the criteria to choose the differentially upregulated and downregulated proteins. A total of 443 differentially expressed proteins were quantified including 162 upregulated proteins and 281 downregulated proteins between the BDEs 4/8th Ger and HOCs group as shown in Table SI. According to the differential expression of proteins and the relationship with cell differentiation, 30 differentially expressed proteins in BDEs 4th/8th Ger and HOCs were further screened, among which 14 were upregulated (fold change >2.0) and 16 were downregulated (fold change <0.5) as shown in Table III. A total of 358 differentially expressed proteins between BDEs 4/8th Ger and HOCs were classified with a heatmap (Fig. 4A). The functional distribution of proteins including their MF, CC and BP was determined by an online tool based on the GO annotation project. Pathway analysis of differentially expressed proteins was elucidated using the KEGG database. Protein-protein interactions were analyzed using STRING. By GO analysis of BP, it was found that most of the differentially expressed proteins were involved in ribonucleoprotein complex biogenesis, blood coagulation, hemostasis, coagulation, wound healing, exocytosis, rRNA processing, ribosome biogenesis, platelet activation and rRNA metabolic process. The majority of the CC proteins have a different distribution, involving collagen-containing extracellular matrix, organellar small ribosomal subunit, mitochondrial small ribosomal subunit, small ribosomal subunit, organellar ribosome, mitochondrial ribosome, cell-substrate junction, focal adhesion, mitochondrial matrix and phagocytic vesicle. According to the analysis of MF, the differentially expressed proteins were categorized into extracellular matrix structural constituent, cell adhesion molecule binding, protein C-terminus binding, integrin binding, phospholipid binding, sulfur compound binding, cargo receptor activity, structural constituent of ribosome, isomerase activity and glycosaminoglycan binding (Fig. 4B). In addition, KEGG analysis indicated that lysosome, phagosome, ECM-receptor interaction, proteoglycans in cancer and tuberculosis were significantly associated with the cell differentiation (Fig. 4C). Furthermore, the protein-protein functional network diagram analysis demonstrated that differentially expressed proteins closely interacted with each other (Fig. 4D).

Discussion

Understanding signaling pathways and molecular regulation of liver regeneration is of high interest, as it provides the basis to improve or modulate the liver regenerative capacity, thus opening new avenues on therapeutic intervention in

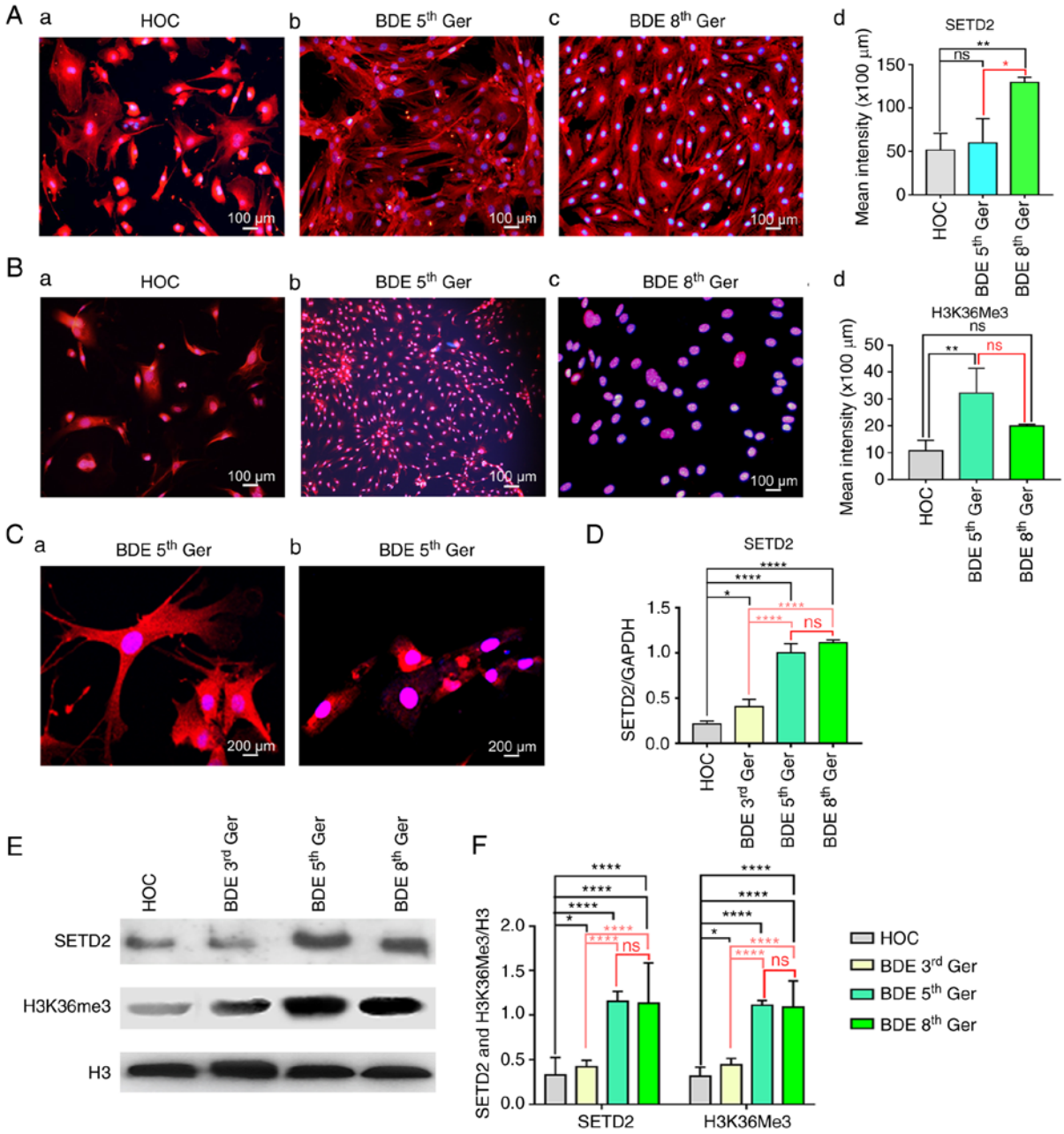

Figure 3. SETD2 and H3K36me3 expression in mice HOCs induced to differentiate into BDEs *in vitro*. Representative images of immunofluorescence staining for (Aa-c) SETD2 and (Ba-c) H3K36me3 with primary HOCs; with the 5th and 8th Ger BDEs represented by the red fluorescence and DAPI used as the counterstain (scale bar, 100 μm) and (A-d, B-d) quantification of red fluorescence. (Ca and b) Confocal microscopy of SETD2 and H3K36me3 in the 5th Ger BDEs (scale bar, 200 μm). (D) The mRNA of SETD2 in the primary HOCs the 5th and 8th Ger BDEs. (E and F) SEDT2 and H3K36me3 in the primary HOCs, the 5th and 8th Ger BDEs. Data presented as mean ± standard deviation, n=3. Black * indicates significant differences vs. primary HOCs; pink * indicates significant differences vs. BDEs 1st Ger and red * indicates significant differences vs. BDEs 5th Ger. ns, P>0.05; *P<0.05; **P<0.01; ****P<0.001. HOCs, hepatic oval cells; BDEs, bile duct epithelial cells; Ger, generation.

liver diseases, other than orthotopic liver transplantation. In the present study, the SEDT2 and H3K36me3 expression in mouse HOCs differentiated into BDEs was studied *in vitro*. The SEDT2 and H3K36me3 antibodies labeled the HOCs and a strong reaction differentiated into the maturation of BDEs was observed. At the same time, HOCs specific marker OV-6 and BDEs marker CK-19 were detected in the differentiation progress to validate the cell types.

HOCs are considered the stem cells in the liver. Under the activation of various factors, HOCs can differentiate into hepatocytes or BDEs. In addition, HOCs can differentiate into pancreatic (19), intestinal epithelial (20), glial (21) and prolactin cells (22) *in vitro* and *in vivo*. At present, most of the studies on the *in vitro* culture model of HOCs focus on the induction of differentiation into hepatocytes, while the induction into BDEs is less studied. Biliary epithelium was previously considered to be a type of simple epithelial cells covering the intrahepatic and extrahepatic bile ducts, whose function is to maintain biliary knots to keep it intact for transporting bile into the intestine. A previous study confirmed that BDEs are not only a group of cells that maintain structural integrity, but also serve an important role in bile secretion, inflammation and

Table III. Detailed information of 38 secreted differential proteins associated with the progress of cell differentiation in HOCs and BDEs 4th Ger and BDEs 8th Ger Groups[a].

Protein	Gene name	Length (kDa)	BDE4th 8th Ger/HOCs ratio	Regulation type
Ninjurin-1	*Ninj1*	152	0.120	Down
cAMP-dependent protein kinase catalytic subunit alpha	*Prkaca*	351	0.668	Down
Interleukin-4 receptor subunit alpha	*Il4r*	810	0.066	Down
Protein NEDD1	*Nedd1*	660	0.668	Down
Protein phosphatase 3 catalytic subunit alpha	*Ppp3ca*	521	0.774	Down
SLAM family member 5	*Slamf5*	329	0.096	Down
Transmembrane anterior posterior transformation protein 1	*Tapt1*	564	0.450	Down
Fibrillin-1	*Fbn1*	2873	0.038	Down
Versican core protein	*Cspg2*	3357	0.022	Down
All-trans-retinol 13,14-reductase	*Retsa*	609	0.265	Down
Calcium-transporting ATPase type 2C member 1	*Atp2c1*	918	0.162	Down
Exopolyphosphatase PRUNE1	*Prune1*	454	0.654	Down
Adipocyte plasma membrane-associated protein	*Apmap*	415	0.532	Down
Fibroblast growth factor 23	*Fgf23*	251	0.017	Down
P2X purinoceptor 4	*P2rx4*	388	0.070	Down
Exostosin-like 3	*Extl3*	918	0.088	Down
Vacuolar protein sorting-associated protein 37B	*Vps37b*	285	2.087	Up
Ubiquitin-conjugating enzyme E2 variant 1	*Ube2v1*	147	1.687	Up
Ubiquitin carboxyl-terminal hydrolase 25	*Usp25*	1055	1.675	Up
Forkhead box protein K1	*Foxk1*	719	2.265	Up
Cleavage and polyadenylation specificity factor subunit 3	*Cpsf3*	684	1.886	Up
Mitogen-activated protein kinase 1	*Mapk1*	358	1.357	Up
RNA-binding protein 15	*Rbm15*	962	1.548	Up
Activating signal cointegrator 1	*Trip4*	581	1.924	Up
Histone-lysine N-methyltransferase SETD2	*Setd2*	2537	4.826	Up
Protein quaking	*Qki*	341	1.425	Up
TBC1 domain family member 1	*Tbc1d*1	1255	1.241	Up
Mesenteric estrogen-dependent adipogenesis protein	*Medag*	303	1.512	Up
SWI/SNF complex subunit SMARCC2	*Smarcc2*	1213	1.550	Up
Protein prune homolog 2	*Prune2*	3084	4.592	Up

[a]Filtered with threshold value of expression fold change >2 and P-value <0.05. HOCs, hepatic oval cells; BDEs, bile duct epithelial cells; Ger, generation.

rejection (4). From the perspective of tissue origin, intrahepatic bile duct is formed by the branch of the portal vein of hepatic precursor cells derived from the liver bud process, while extrahepatic bile duct is formed by the endodermal cells between the liver bud process and the ventral pancreatic process (23). At present, the tissue origin and differentiation process of BDEs remain to be elucidated, but some studies suggest that the biliary system, liver and pancreas are also derived from the endodermal foregut during embryofetal development. In the extrahepatic bile duct, there are a large number of peribiliary glands and there are a subgroup of SOX17+/PDX1-fine cells in these glands, which could differentiate into extrahepatic BDEs (24). In the present study, the *in vitro* induction system was successfully established by inducing the *in vitro* cultured HOCs to differentiate into BDEs through a variety of cytokines. The extraction of HOCs in mice was explored by using 10 μg EGF + 5 μg SCF + 5 μg LIF protocol to BDEs induced directional differentiation. In this induction system, EGF is a mitogenic factor. EGF plays a role in promoting cell proliferation by binding to its membrane receptor EGFR. In the study, EGF was used in rats after 2AAF/PH. It has been confirmed that EGF can promote the proliferation of bile duct cells and their surrounding cells and promote the migration of HOCs from the portal area to the liver parenchyma (25). In addition, SCF is an important hematopoietic stimulator, which activates and proliferates cells by binding to c-kit on the cell surface. c-kit can be expressed on the surface of HOCs and SCF may play a key role in the proliferation and activation of oval cells (26). Through the effect of EGF and SCF, mice HOCs were successfully induced to differentiate into BDEs expressing CK-19 and the morphology of the cells was significantly changed, which was in line with the morphological

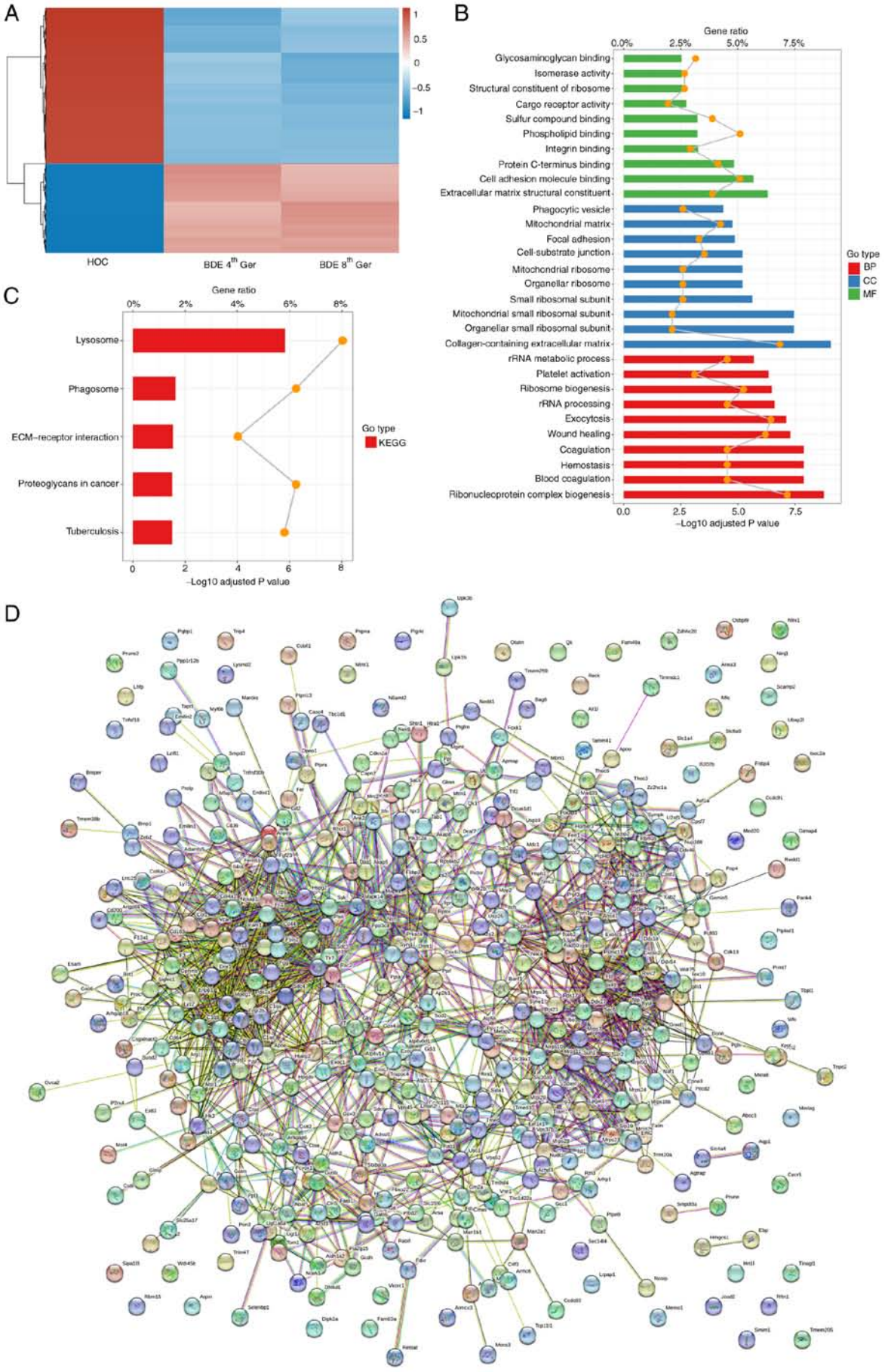

Figure 4. Bioinformatics analysis of 443 differentially expressed proteins. (A) Heatmap; (B) GO analysis; biological process, cellular component and molecular function. (C) KEGG pathway analysis and (D) Protein-protein functional network using the STRING tool. GO, Gene Ontology; BP, biological process; CC, cellular component; MF, molecular function; KEGG, Kyoto Encyclopedia of Genes and Genomes.

characteristics of epithelial cells (Fig. 1A-I) and the expression of CK-19 (Fig. 2A-D and Table II) in cultured cells was confirmed by immunofluorescence and flow cytometry. It is suggested that the induction protocol can be used to induce HCOs to differentiate into mature BDEs *in vitro* with stability and reliability.

The bivalent domains, consisting of active modification H3K4me3 and repressive modification H3K27me3, have been shown to play an important role in the mechanism of action of histone modification proteins in stem cells (27). Functional analyses of these molecules during liver development have advanced the understanding of several complex chromatin-modifying enzymes involved in cell lineage commitment (28,29). In addition, it is reported that expression of liver-specific transcription factors is changed by administration of histone deacetylase inhibitors *in vitro* (30). Special attention is being paid to their role in controlling both growth and differentiation of stem cells *in vitro*. In past decades, the study of H3K36me3 and SETD2 mainly focus on their function as tumor suppressors, including clear cell renal cell carcinoma, chondroblastomas, lymphoma, acute leukemia, intestinal tumorigenesis and so on (31-35). In the mechanism, SETD2, H3K36 histone methyltransferase in yeast, has been reported to be required for transcription elongation (36). Also, SETD2 could directly regulate transcriptional initiation of Fgfr3 through histone H3K36me3 modification (37). In the present study, SETD2 could regulate H3k36Me3 expression to promote the HOCs committed into BDEs. Regretfully, although SETD2 and H3K36me3 were studied in the progress of HOCs differentiation into BDEs knockdown SEDT2 mice were not established. Were this performed, it could be observed that HOCs simply maintained their original state and failed to form mature BDEs. Therefore, it is hypothesized that SETD2 can regulate the expression of H3K36me3 and promote the differentiation of HOCs into BDEs.

Protein detection plays an important role in biological and biomedical sciences. With the development and improvement of label-free quantitative proteomics technology, it is possible to study diseases from the whole protein expression level of body fluids, tissues or cells which can reflect the disease state of the body so as to provide new specific molecular markers for early diagnosis of disease and new clues for understanding the pathogenesis of the disease. In the present study, this technology was used to detect the proteomic through the differentiation of HOCs induced into BDEs. Unexpectedly, SETD2 matched the label-free proteins test and experienced a 4.826 ratio change with more BDE4th 8th Ger than HOCs (Table III). The whole trend in change was consistent with the cell morphological features. In addition, in the 30 differentially expressed proteins associated with cell differentiation, it was found that, after using NCBI functional annotation(https://www.ncbi.nlm.nih.gov/), the 30 differentially expressed proteins in HOCs directional differentiation to the process of BDEs involved in sugar metabolism, angiogenesis, transcriptional regulation, histone modification, cell cycle regulation, chromatin regulation, bile metabolism and a series of important steps in cell differentiation (Table SII). Thus, it was found that most of the proteins in HOCs were committed to differentiation into BDEs with multi-function coordination working. In addition, some of the proteins are also of importance in liver function adjustment, such as lipid metabolism. Thus, they can be identified as the progress of HOCs differentiation into BDEs. Epigenetic modifying proteins can promote original cells to be other mature cells accompanied by the formation of the metabolism function. There is also research reporting the essential role of SETD2 and H3K36me3 in cell differentiation, such as bone marrow mesenchymal stem cells (18), fetal erythropoiesis (38), hematopoietic stem cell (17), osteosarcoma cells (39), bone regeneration (40), germline stem cells (41), human epidermal stem cells and human epidermal stem cells (42). There is also research showing the proteomic in hepatic stem cells (43,44), although this examined only cell membrane and cytoplasmic proteins, but not nuclear proteins, which play an important role in differentiation. The proteomics of HOCs differentiating into BDEs has not been studied. The proteomic study of the present study can provide a good basis for the future study of BDEs.

However, the present study is still subject to some flaws. SETD2 knockdown mice were not constructed, making it difficult to directly observe how SETD2 adjusts H3K36me3 in the progress of HOCs committed differentiation into BDEs. In further research, SETD2 knockdown and overexpression mice will be chosen to study the relationship between SETD2 and H3K36me3 in HOCs differentiation into BDEs. Continuous efforts will be made to study this and make the present hypothesis more convincing. Additionally, the hub proteins will be explored with a label-free proteins test to clarify the significance of epigenetic modification proteins in hepatic oval cell differentiation.

In summary, the present study demonstrated the way SETD2 regulates H3K36me3, a critical factor in the differentiation of HOCs and is endowed with significant research potential for the dry maintenance and differentiation of liver oval cells into BDEs, which can be used in stem cell research for biliary diseases, bile duct repair, liver transplantation and other clinical applications.

Acknowledgements

Not applicable.

Founding

The present study was supported by PhD research start-up funds of Dali University, Dali, Yunnan, P.R. China (grant no. KYBS201720).

Availability of data and materials

The datasets used and/or analyzed during the current study are available from the corresponding author on reasonable request.

Authors' contributions

YC initiated the research and drafted the manuscript; LJ drafted the manuscript and completed all experiments; LJ and YC confirm the authenticity of all the raw data. ZS and SH analyzed the data and assisted in preparing the manuscript; YT provided practical technical guidance and analyzed the data; and IM checked the language issues and assisted in the experiments. All authors read and approved the final manuscript.

Ethics approval and consent to participate

The Biomedical Research Ethics Committee of the School of Medicine at Dali University approved the present study [approval number: SYXK(yunnan)2018-0002].

Patient consent for publication

Not applicable.

Competing interests

The authors declare that they have no competing interests.

References

1. Carpino G, Cardinale V, Renzi A, Hov JR, Berloco PB, Rossi M, Karlsen TH, Alvaro D and Gaudio E: Activation of biliary tree stem cells within peribiliary glands in primary sclerosing cholangitis. J Hepatol 63: 1220-1228, 2015.
2. Miyajima A, Tanaka M and Itoh T: Stem/progenitor cells in liver development, homeostasis, regeneration, and reprogramming. Cell Stem Cell 14: 561-574, 2014.
3. Alison MR, Poulsom R and Forbes SJ: Update on hepatic stem cells. Liver 21: 367-373, 2001.
4. Lowes KN, Croager EJ, Olynyk JK, Abraham LJ and Yeoh GC: Oval cell-mediated liver regeneration: Role of cytokines and growth factors. J Gastroenterol Hepatol 18: 4-12, 2003.
5. Fujikawa T, Hirose T, Fujii H, Oe S, Yasuchika K, Azuma H and Yamaoka Y: Purification of adult hepatic progenitor cells using green fluorescent protein (GFP)-transgenic mice and fluorescence-activated cell sorting. J Hepatol 39: 162-170, 2003.
6. Alison M, Golding M, Lalani el-N and Sarraf C: Wound healing in the liver with particular reference to stem cells. Philos Trans R Soc Lond B Biol Sci 353: 877-894, 1998.
7. Akhurst B, Croager EJ, Farley-Roche CA, Ong JK, Dumble ML, Knight B and Yeoh GC: A modified choline-deficient, ethionine-supplemented diet protocol effectively induces oval cells in mouse liver. Hepatology 34: 519-522, 2001.
8. Dabeva MD and Shafritz DA: Activation, proliferation, and differentiation of progenitor cells into hepatocytes in the D-galactosamine model of liver regeneration. Am J Pathol 143: 1606-1620, 1993.
9. Factor VM, Radaeva SA and Thorgeirsson S: Origin and fate of oval cells in dipin-induced hepatocarcinogenesis in the mouse. Am J Pathol 145: 409-422, 1994.
10. Tatematsu M, Kaku T, Medline A and Farber E: Intestinal metaplasia as a common option of oval cells in relation to cholangiofibrosis in liver of rats exposed to 2-acetylaminofluorene. Lab Invest 52: 354-362, 1985.
11. Wright N, Samuelson L, Walkup MH, Chandrasekaran P and Gerber DA: Enrichment of a bipotent hepatic progenitor cell from naïve adult liver tissue. Biochem Biophys Res Commun 366: 367-372, 2008.
12. Yoon BI, Choi YK and Kim DY: Differentiation processes of oval cells into hepatocytes: Proposals based on morphological and phenotypical traits in carcinogen-treated hamster liver. J Comp Pathol 131: 1-9, 2004.
13. Yin L, Lynch D, Ilic Z and Sell S: Proliferation and differentiation of ductular progenitor cells and littoral cells during the regeneration of the rat liver to CCl4/2-AAF injury. Histol Histopathol 17: 65-81, 2002.
14. Park HJ, Choi YJ, Kim JW, Chun HS, I'm I, Yoon S, Han YM, Song CW and Kim H: Differences in the epigenetic regulation of cytochrome P450 genes between human embryonic stem cell-derived hepatocytes and primary hepatocytes. PLoS One 10: e0132992, 2015.
15. Kanayama K, Chiba T, Oshima M, Kanzaki H, Koide S, Saraya A, Miyagi S, Mimura N, Kusakabe Y, Saito T, *et al*: Genome-wide mapping of bivalent histone modifications in hepatic stem/progenitor cells. Stem Cells Int 2019: 9789240, 2019.
16. Livak KJ and Schmittgen TD: Analysis of relative gene expression data using real-time quantitative PCR and the 2(-Delta Delta C(T)). Methods 25: 402-408, 2001.
17. Zhang YL, Sun JW, Xie YY, Zhou Y, Liu P, Song JC, Xu CH, Wang L, Liu D, Xu AN, *et al*: Setd2 deficiency impairs hematopoietic stem cell self-renewal and causes malignant transformation. Cell Re 28: 476-490, 2018.
18. Wang L, Niu N, Li L, Shao R, Ouyang H and Zou W: H3K36 trimethylation mediated by SETD2 regulates the fate of bone marrow mesenchymal stem cells. PLoS Biol 16: e2006522, 2018.
19. Li Y, Zhao LJ, Xia FZ, Li YX and Lu YL: Transdifferentiation of hepatic oval cells into pancreatic islet beta-cells. Front Biosci (Landmark Ed) 17: 2391-2395, 2012.
20. Barut V and Sarraf CE: Intestinal metaplasia in liver of rats after partial hepatectomy and treatment with acetylaminofluorene. Cell Prolif 42: 657-560, 2009.
21. Deng J, Steindler DA, Laywell ED and Petersen BE: Neural trans-differentiation potential of hepatic oval cells in the neonatal mouse brain. Exp Neurol 182: 373-382, 2003.
22. Lee EJ, Russell T, Hurley L and Jameson JL: Pituitary transcription factor-1 induces transient differentiation of adult hepatic stem cells into prolactin-producing cells in vivo. Mol Endocrinol 19: 964-971, 2005.
23. Raynaud P, Carpentier R, Antoniou A and Lemaigre FP: Biliary differentiation and bile duct morphogenesis in development and disease. Int J Biochem Cell Biol 43: 245-256, 2011.
24. Carpino G, Cardinale V, Onori P, Franchitto A, Berloco PB, Rossi M, Wang Y, Semeraro R, Anceschi M, Brunelli R, *et al*: Biliary tree stem/progenitor cells in glands of extrahepatic and intraheptic bile ducts: An anatomical in situ study yielding evidence of maturational lineages. J Anat 220: 186-199, 2012.
25. Nagy P, Bisgaard H, Santoni-Rugiu E and Thorgeirsson SS: In vivo infusion of growth factors enhances the mitogenic response of rat hepatic ductal (oval) cells after administration of 2-accetylaminofluorene. Hepatology 23: 71-79, 1996.
26. Matsusaka S, Tsujimura T, Toyosaka A, Nakasho K, Sugihara A, Okamoto E, Uematsu K and Terada N: Role of c-kit receptor tyrosine kinase in development of oval cells in the rat 2-acetylaminofluorene/partial hepatectomy model. Hepatology 29: 670-676, 1999.
27. Stock JK, Giadrossi S, Casanova M, Brookes E, Vidal M, Koseki H, Brockdorff N, Fisher AG and Pombo A: Ring1-mediated ubiquitination of H2A restrains poised RNA polymerase II at bivalent genes in mouse ES cells. Nat Cell Biol 9: 1428-1435, 2007.
28. Xu CR, Cole PA, Meyers DJ, Kormish J, Dent S and Zaret KS: Chromatin 'prepattern' and histone modifiers in a fate choice for liver and pancreas. Science 332: 963-966, 2011.
29. Aoki R, Chiba T, Miyagi S, Negishi M, Konuma T, Taniguchi H, Ogawa M, Yokosuka O and Iwama A: The polycomb group gene product Ezh2 regulates proliferation and differentiation of murine hepatic stem/progenitor cells. J Hepatol 52: 854-863, 2010.
30. Kubicek S, Gilbert JC, Fomina-Yadlin D, Gitlin AD, Yuan Y, Wagner FF, Holson EB, Luo T, Lewis TA, Taylor B, *et al*: Chromatin-targeting small molecules cause class-specific transcriptional changes in pancreatic endocrine cells. Proc Natl Acad Sci USA 109: 5364-5369, 2012.
31. Fang D, Gan H, Lee JH, Han J, Wang Z, Riester SM, Jin L, Chen J, Zhou H, Wang J, *et al*: The histone H3.3K36M mutation reprograms the epigenome of chondroblastomas. Science 352: 1344-1348, 2016.
32. Yuan H, Li N, Fu D, Ren J, Hui J, Peng J, Liu Y, Qiu T, Jiang M, Pan Q, *et al*: Histone methyltransferase SETD2 modulates alternative splicing to inhibit intestinal tumorigenesis. J Clin Invest 127: 3375-3391, 2017.
33. Moffitt AB, Ondrejka SL, McKinney M, Rempel RE, Goodlad JR, Teh CH, Leppa S, Mannisto S, Kovanen PE, Tse E, *et al*: Enteropathy-associated T cell lymphoma subtypes are characterized by loss of function of SETD2. J Exp Med 214: 1371-1386, 2017.
34. Zhu X, He F, Zeng H, Ling S, Chen A, Wang Y, Yan X, Wei W, Pang Y, Cheng H, *et al*: Identification of functional cooperative mutations of SETD2 in human acute leukemia. Nat Genet 46: 287-293, 2014.
35. Duns G, van den Berg E, van Duivenbode I, Osinga J, Hollema H, Hofstra RM and Kok K: Histone methyltransferase gene SETD2 is a novel tumor suppressor gene in clear cell renal cell carcinoma. Cancer Res 70: 4287-4291, 2010.
36. Zhang Y, Xie S, Zhou Y, Xie Y, Liu P, Sun M, Xiao H, Jin Y, Sun X, Chen Z, *et al*: H3K36 histone methyltransferase Setd2 is required for murine embryonic stem cell differentiation toward endoderm. Cell Rep 8: 1989-2002, 2014.

37. Li J, Moazed D and Gygi SP: Association of the histone methyltransferase Set2 with RNA polymerase II plays a role in transcription elongation. J Biol Chem 277: 49383-49388, 2002.
38. Li Y, Tang H, Chen F, Chen J, Wang H, Chen Z, Duan Y, Wang X, Li L and Ouyang K: SETD2 is essential for terminal differentiation of erythroblasts during fetal erythropoiesis. Biochem Biophys Res Commun 552: 98-105, 2021.
39. Jiang C, He C, Wu Z, Li F and Xiao J: Histone methyltransferase SETD2 regulates osteosarcoma cell growth and chemosensitivity by suppressing Wnt/β-catenin signaling. Biochem Biophys Res Commun 502: 382-388, 2018.
40. Jia X, Long Q, Miron RJ, Yin C, Wei Y, Zhang Y and Wu M: Setd2 is associated with strontium-induced bone regeneration. Acta Biomater 53: 495-505, 2017.
41. McCarthy A, Sarkar K, Martin ET, Upadhyay M, Jang S, Williams ND, Forni PE, Buszczak M and Rangan P: Msl3 promotes germline stem cell differentiation in female Drosophila. Development 149: dev199625, 2022.
42. Rinaldi L, Datta D, Serrat J, Morey L, Solanas G, Avgustinova A, Blanco E, Pons JI, Matallanas D, Von Kriegsheim A, *et al*: Dnmt3a and Dnmt3b associate with enhancers to regulate human epidermal stem cell homeostasis. Cell Stem Cell 19: 491-501, 2016.
43. Montaldo C, Mancone C, Conigliaro A, Cozzolino AM, de Nonno V and Tripodi M: SILAC labeling coupled to shotgun proteomics analysis of membrane proteins of liver stem/hepatocyte allows to candidate the inhibition of TGF-beta pathway as causal to differentiation. Proteome Sci 12: 15, 2014.
44. Hurrell T, Segeritz CP, Vallier L, Lilley KS and Cromarty AD: A proteomic time course through the differentiation of human induced pluripotent stem cells into hepatocyte-like cells. Sci Rep 9: 3270, 2019.